An Investigation of the Potentialities of the Electromagnetic Frequency Regulator

Ariel S.L. Patriota * **Ricardo F. Pinheiro** ** **Gabriel I. Medina T.** ***

* *Master's Program in Electrical Energy, Federal University of Rio Grande do Norte, Natal, RN (e-mail: ariel.patriota.837@ufrn.edu.br).*
** *Department of Computer Engineering and Automation, Federal University of Rio Grande do Norte, Natal, RN (e-mail: ricardo.pinheiro@ufrn.br)*
*** *Department of Mechanical Engineering, Federal University of Rio Grande do Norte, Natal,RN (e-mail: gabriel.medina@ufrn.br)*

Abstract: This work analyzes the Electromagnetic Frequency Regulator (EFR) when used in a wind power system with hybridization of energy sources. The study was conducted through numerical simulation on Scilab platform. The conventional mechanical transmission (gearbox) was substituted by a hydrostatic system (pump and motor). Feedback linearization was used to control the motor's displacement, and a prediction algorithm was developed to compute the reference steady-state angular speeds of the EFR's armature and the rotating electromagnetic field. The results indicated that the EFR can effectively supply the generator load regardless of the wind speed. It was also shown that electrical energy can be accumulated in batteries during regimes of wind speeds higher than a reference set-point, to be used when the harnessed wind power is lower than the load. This shows that the EFR is a viable hybridization solution to wind energy systems, ensuring the highest levels of power quality.

Keywords: Electromagnetic Frequency Regulator (EFR), Wind turbines, Variable load, Induction machine.

1. INTRODUCTION

Modern variable-speed wind turbines rely on electronic conversion systems to attach the generator to the grid. They operate on a voltage-dependent basis and can be disconnected because of some malfunction. Many of such topologies utilize doubly fed induction generators (DFIG) or multipolar synchronous generators. The first group needs some mechanical coupling (gearbox) between the turbine and the generator, while the second does not need it because of the high pole number. Both solutions require voltage source converter (VSC) modules between the generator and the grid. This can impair power quality as well as make isolated operation unfeasible. Furthermore, the gearbox represents a constant source of noise and fatigue issues.

Recent ideas have emerged to overcome the gearbox problems by substituting this connection with hydraulic systems, *e.g.*: (1) the Delft Offshore Turbine (Delft, 2020); (2) a transmission patented by Norwegian company ChapDrive (Frøyd, 2009; Thomsen et al., 2012); and (3) a proposal made by Flesch (2012) that allies a hydrostatic circuit to a PID controller and a synchronous generator.

Two desirable features are open to improvement in such conceptions: (1) operating the systems isolated from the grid in case of emergency or by design; and (2) implementing an energy hybridization scheme with sinergy of different sources, to obtain a more stable and reliable performance (Silva, 2015, p. 10).

The Electromagnetic Frequency Regulator (EFR) has appeared in the context of hybridized energy sources. An adaptation of the classic induction motor, it has been studied by Silva et al. (2015a,b,c). In 2021, a Brazilian patent registration was released for this device, described as a "variable speed aerogenerator of constant voltage and frequency, with electromagnetic frequency regulation" (Pinheiro et al., 2021). The combination EFR–generator delivers an electrical wave free of harmonics. Besides the positive effects on the energy quality, it offers a solution to the problem of operating a system isolated from the grid.

1.1 Presentation of the Technology

The Electromagnetic Frequency Regulator is a squirrel-cage induction machine electrically fed by a VSC (Fig. 1).

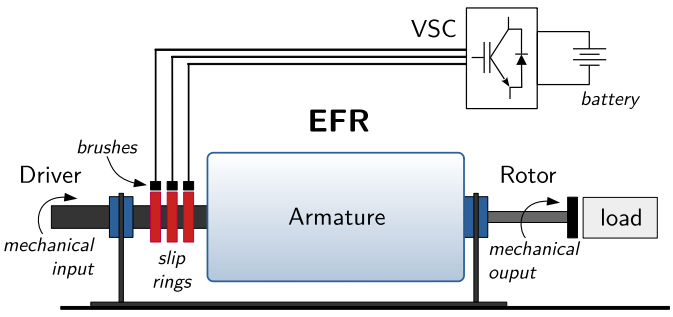

Figure 1: Schematic diagram of the EFR

Some features of the EFR are worth mentioning:

(1) The component that corresponds to the conventional stator is supported on bearings and can rotate freely; it is, for the sake of simplification, called the armature.
(2) The armature rotates together with a mechanical driver (*e.g.,* a wind turbine). Slip rings placed on the armature shaft provide electrical contact of the VSC with the armature windings.
(3) The interaction of the EFR rotor with the armature is more complex than that of a conventional motor: the VSC adjusts the speed of the electromagnetic rotating field to the variable angular speed of the armature to keep the rotor speed output in a reference level, in response to the wind power fluctuations. This requires a bidirectional VSC to provide field rotation in any direction.
(4) The VSC is energized by a supplementary source (like a battery fed by photovoltaic panels), which permits it to draw power from the battery in periods of low wind activity, and, otherwise, to direct the surplus wind power into the battery. The machine is therefore naturally apt for hybridization.

1.2 Recent Literature Survey

Costa et al. (2016a; 2016b) designed a wind energy system involving the hybridization of a wind turbine with photovoltaic panels and an EFR, having focused on sizing the system to meet the consumers' requirements without going into details about the effects of the availability of the energy sources on the EFR operation. Silva et al. (2015a,c) demonstrated the feasibility of the EFR as a suitable equipment for speed control between the turbine and the synchronous generator. His Ph.D. thesis (2015) showed it experimentally. Ramos's doctoral work (2019), building upon Silva's text, showed that the EFR can be successfully applied to a big wind turbine that has an induction generator connected to the grid. He has also shown that the EFR smoothes out mechanical oscillations caused by wind, which contributes to increasing the gear multiplier's service life. In another text Ramos et al. (2019) analyzed the application of the EFR in a large wind energy system, emphasizing the dynamic control of the maximum power extracted from the wind (MPPT).

Freitas Nunes (2021) showed that the adoption of a fuzzy control strategy to ensure constant speed of a generator associated with the EFR improves performance, when compared to the initial proposal of Silva. Moreover, a paper by J. Silva et al. (2021), analyzing the harmonics impact of a wind turbine in a squirrel-cage induction generator (SCIG) project driven by an EFR, pointed out that not only the system inertia but also the responsive electromagnetic control of mechanical oscillations contribute to mitigating the harmonics effects on the grid. The study also demonstrated that the EFR yields a better performance when it comes to injection of harmonics, if compared to DFIG.

You et al. (2013) introduced a similar topology of an induction machine with no stationary parts, named "Electromagnetic Coupler" (EMC). Although both designs aim to create a mechanical coupling between the turbine and the generator, there are noticeable similarities and differences between the conceptual approaches: (1) The high-speed shaft of the induction machine, in the two cases, is usually connected to a synchronous generator, but the EFR may be associated to an induction generator as well. (2) The EFR's VSC is DC/AC and needs a connection to an external DC power source, which opens the way to hybridization. The EMC, however, uses a back-to-back converter that depends on AC power from the grid.

1.3 Scope and Conditions

This text presents a computational study that investigates a way of harnessing wind energy where the EFR works as an intermediate conversion device between the turbine and the generator, and the main mechanical transmission is performed by a hydrostatic circuit consisting of a volumetric pump (▲) and a hydraulic motor (▼) (cf. the arrangement of Fig. 2).

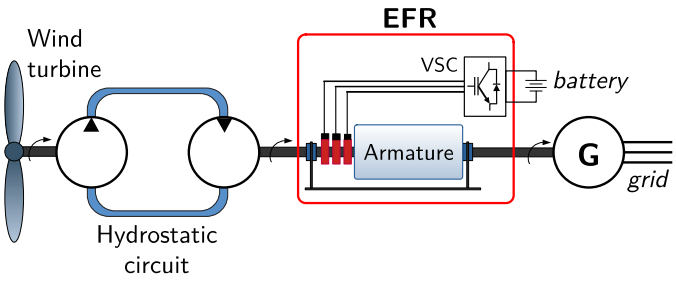

Figure 2: Layout of this study: turbine – transmission – EFR – generator

The following conditions apply:

(1) The EFR and its VSC are electrically isolated from the grid.
(2) The pump has a fixed displacement (the volume of liquid pushed per shaft revolution), while the motor's displacement is variable. Controlling this latter parameter will generate a variable-torque transmission given by
$$T_a = \eta_m \, d\Delta p, \tag{1}$$
where T_a is the torque delivered to the armature, η_m is the motor's mechanical efficiency, d is its displacement and Δp is the line pressure load.
(3) The control strategies for the hydrostatic transmission and the VSC are distinct.
(4) The generator (G) is directly connected to the grid. The reference here is to the synchronous generator, but the idea also applies to the asynchronous model (Ramos et al., 2019).

This hybridized scheme comprises a hydromechanical part (turbine and transmission) and an electromechanical part (EFR, generator and supplementary energy source).

1.4 Methodology

Based on the induction machine theory, the dynamic equations of the EFR will be elaborated. The rotor slip is calculated through a dynamic frame generalization. This advances beyond previous works (Ramos et al., 2019; Silva, 2015) that adopted a static reference frame (the Earth).

Two contributions result from the study, following the order of appearance in the text:

- a prediction algorithm for the steady state of the EFR system when working between two boundary conditions, namely: the wind power (input) and the generator load (output);
- a control strategy model adapted to the wind fluctuations.

A Scilab program was written to simulate the machine behavior in two scenarios (one simpler and the other generalized) of wind speed and load profile. The goal here is not to discuss details such as transients, but to grasp a general understanding of the EFR performance in terms of its ability (and limitations) to convert mechanical energy when working in a hybrid arrangement like the one proposed in Fig. 2.

1.5 Purpose and Importance of the Study

The EFR offers a hybridization alternative with potential applications in contexts where the use of the conventional gearbox proves to be unfeasible or difficult to implement. This work proposes that the combination of a hydrostatic transmission (a well-known technology) to the EFR, an innovative project, in hybridization with a secondary energy source to compose a wind energy generation topology, brings many benefits to the existing generation schemes. Some advantages of this arrangement will be shown in the text, and it is expected that more applications for the EFR will emerge in the future.

2. DYNAMIC ANALYSIS

Let T_a be the torque applied by the hydraulic motor on the EFR armature; T_e, the electromagnetic torque transmitted to the EFR rotor through the air gap; and T_r, the resistant load torque. The mass moments of inertia of the EFR armature and rotor are J_a and J_r.The angular velocities involved are:

- ω_a, the absolute angular speed of the armature;
- ω_i, the angular speed of the rotating electromagnetic field produced by the armature currents and generated in the armature windings — This text considers the mechanical angular speed of the rotating field, by defining $\omega_i = \omega_i^{\text{ele}}/\text{pp}$, where pp is the EFR pole pair number, $\omega_i^{\text{ele}} = 2\pi f$ and f is the frequency of the currents;
- $\omega_e = \omega_a + \omega_i$, the absolute angular speed of the rotating field; and
- ω_r, the absolute angular speed of the rotor.

Fig. 3 shows a dynamic representation of the main EFR components as well as their absolute and relative speeds.

An observer at the armature, Fig. 3b, sees the rotating field moving away at rate ω_i, regardless of the armature's motion indicated by ω_a. The angular speed of the rotor with respect to the armature is $\omega_r - \omega_a$.

The rotor **internal slip** is defined as

$$s = \frac{\omega_i - (\omega_r - \omega_a)}{\omega_i} = \frac{\omega_a + \omega_i - \omega_r}{\omega_i}. \tag{2}$$

That is, the internal slip is calculated from the perspective of a dynamic reference frame, R_1, instead of the classic static, Earth-centered referential R_0.

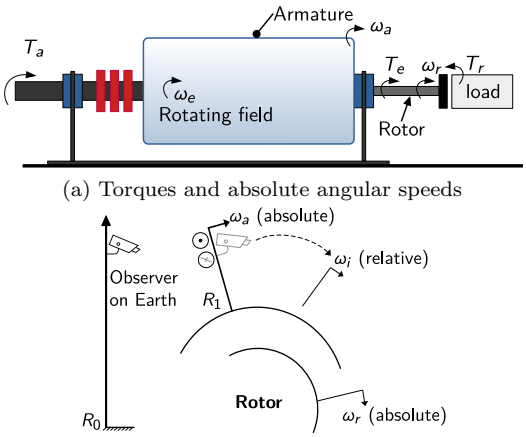

(a) Torques and absolute angular speeds

(b) Fixed (R_0) and Mobile (R_1) reference frames

Figure 3: Dynamic variables of main EFR components

The **external or apparent slip**, evaluated from the Earth, is

$$s_0 = \frac{\omega_a + \omega_i - \omega_r}{\omega_a + \omega_i}, \tag{3}$$

giving $s = s_0\,(1 + \omega_a/\omega_i)$. If $\omega_a = 0$, then $s = s_0$ (conventional induction machine) and reference frames R_0 and R_1 overlap and coincide. Everything happens, therefore, as if the armature were blocked, the rotating field had absolute angular speed ω_i and the rotor had absolute angular speed given by $\omega_r - \omega_a$.

The dynamic equations for the rotor and the armature are:

$$J_a\dot{\omega}_a = T_a - T_e - T_{fa}, \tag{4}$$
$$J_r\dot{\omega}_r = T_e - T_r - T_{fr}, \tag{5}$$

where T_{fa}, T_{fr} are friction torques given by: $T_{fa} = B_a\omega_a$, $T_{fr} = B_r\omega_r$, and B_a, B_r are friction coefficients.

The electromagnetic torque is modeled in classical theory (Umans, 2014, p. 361) in terms of equivalent circuit parameters of the induction motor:

$$T_e = \frac{1}{\omega_i}\frac{qV_{1\text{eq}}^2 R_2/s}{(R_{1\text{eq}} + R_2/s)^2 + (X_{1\text{eq}} + X_2)^2}, \tag{6}$$

where q is the number of phases, indices 1 and 2 refer to the armature and to the rotor respectively, s is the internal slip and the *eq*-variables — voltage (V), resistance (R) and reactance (X) — are given by the Thèvenin equivalents of the circuit: being X_m the magnetizing reactance (referred to the armature), the parameters are:

$$V_{1\text{eq}} = \left|\frac{V}{\sqrt{3}}\frac{\jmath X_m}{R_1 + \jmath(X_1 + X_m)}\right|, \tag{7}$$
$$Z_{1\text{eq}} = \frac{\jmath X_m(R_1 + \jmath X_1)}{R_1 + \jmath(X_1 + X_m)}, \tag{8}$$
$$R_{1\text{eq}} = \text{Re}(Z_{1\text{eq}}), \tag{9}$$
$$X_{1\text{eq}} = \text{Im}(Z_{1\text{eq}}). \tag{10}$$

3. STEADY-STATE ANALYSIS

The purpose of this section is to determine the equilibrium state (speeds, powers, slip) of the set: EFR–hydrostatic transmission–load by means of a dynamic energy balance.

The mechanical power output P_m due to the EFR is given by the product of the electromagnetic power $T_e\omega_i$, (6), by $1 - s$:

$$P_m = \frac{(1-s)\,qV_{1\text{eq}}^2 R_2/s}{(R_{1\text{eq}} + R_2/s)^2 + (X_{1\text{eq}} + X_2)^2}. \tag{11}$$

Eq. (11) is satisfied by two possible slips $s = (a \pm b)/c$, where

$$a = qV_{1\text{eq}}^2 - 2P_m R_{1\text{eq}}, \tag{12}$$

$$b = \sqrt{q^2 V_{1\text{eq}}^4 - 4P_m \left[P_m (X_{1\text{eq}} + X_2)^2 + qV_{1\text{eq}}^2 (R_{1\text{eq}} + R_2)\right]} \tag{13}$$

$$c = 2\left\{P_m \left[R_{1\text{eq}}^2 + (X_{1\text{eq}} + X_2)^2\right]/R_2 + qV_{1\text{eq}}^2\right\}. \tag{14}$$

The root that makes physical sense here is the one with the lowest absolute value (Ramos et al., 2019, p. 77). In general, given two numbers x and y, this is evaluated by taking $\frac{1}{2}\left(x + y - |x-y| \cdot \frac{|x+y|}{x+y}\right)$. Applied to the slip, it follows that the steady-state value of s, written s^*, is:

$$\begin{aligned} s^* &= \frac{a+b+a-b}{2c} - \left|\frac{a+b-a+b}{2c}\right| \cdot \frac{|a+b+a-b|/|c|}{(a+b+a-b)/c} \\ &= \frac{a}{c} - \left|\frac{b}{c}\right| \cdot \frac{|a|}{a} \cdot \frac{c}{|c|}. \end{aligned} \tag{15}$$

As $|a|/a = \operatorname{sgn}(a)$, $b \geqslant 0$ and $|c|^2 = c^2$, it gives

$$s^* = \frac{a - \operatorname{sgn}(a)\, b}{c}. \tag{16}$$

The equivalent impedances depend on the frequency and consequently on s, then a, b and c will also, in the end, depend on s. That rises a circular problem. One way to handle it is computing a, b and c by starting with $s = 0$ and iterating until $s \to s^*$ with negligible error.

From reactance values X_1^0, X_2^0 and X_m^0 measured in laboratory tests for a particular frequency f_0 (corresponding to a speed ω_i^0), one can extrapolate to other frequencies by calculating, for a new speed ω_i:

$$[X_1 \;\; X_2 \;\; X_m] = \frac{\omega_i}{\omega_i^0}\left[X_1^0 \;\; X_2^0 \;\; X_m^0\right]. \tag{17}$$

Saturation effects are being neglected with this assumption.

The mechanical power P_r delivered to the load is the sum of the mechanical power P_a that comes to the armature from the hydraulic motor plus the mechanical power P_m properly supplied by the VSC (11) minus losses (due to the friction torques $T_f = B\omega$, hence the dissipated power P_L can be written as $\sum T_f \cdot \omega = B_a\omega_a^2 + B_r\omega_r^2$). The balance is equated as:

$$P_r = P_m + P_a - B_a\omega_a^{*2} - B_r\omega_r^{*2}, \tag{18}$$

where ω_a^* is the steady-state value of ω_a, given implicitly by

$$\omega_a^* = \frac{P_a}{T_a^*} = \frac{P_a}{T_r + B_a\omega_a^* + B_r\omega_r^*}. \tag{19}$$

The mechanical power of (11) can be found by isolating P_r in (18), and variables a, b and c are evaluated at each interaction of s until one finds a satisfactory numerical solution for s^* and, consequently, for ω_a^* and ω_i^*. These two outputs will be the inputs to the two control strategies for, respectively, the hydraulic motor's displacement ($\mathrm{d_M}$,) and the frequency (ω_i) of the currents injected by the VSC into the armature. The Slip algorithm (Fig. 4) organizes this sequence of steps.

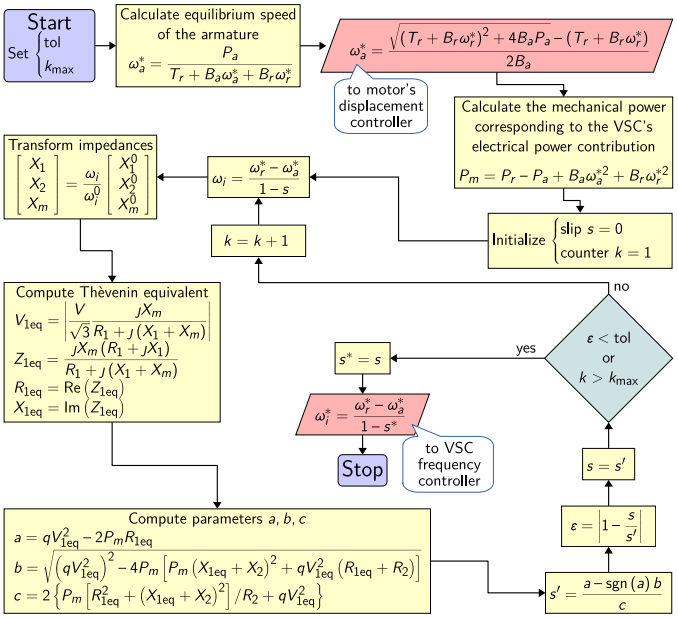

Figure 4: **Slip algorithm**: determination of the steady-state slip for the EFR when operating at input power P_a and output power P_r

An overview of the control system, including interrelations between electrical and mechanical parts, is shown in Fig. 5.

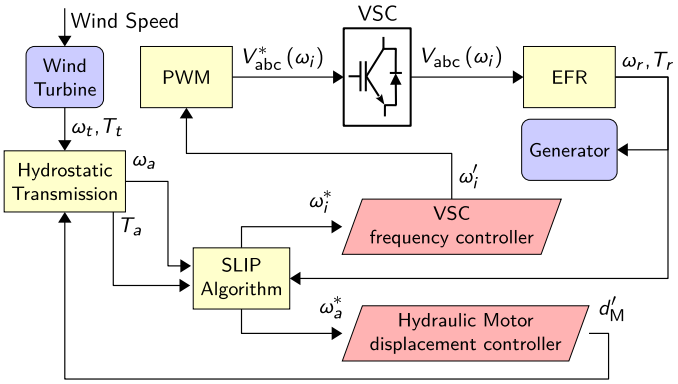

Figure 5: Logic diagram of the system

The wind information goes to the hydrostatic transmission in the form of a speed ω_t and a torque T_t. The transmission (more specifically the hydraulic motor) updates the motor's displacement d_M to a new d'_M, commanded by the displacement controller. The transmission outputs are: the EFR armature speed ω_a and its respective torque T_a, according to (1). These parameters are passed to the Slip algorithm (Fig. 4) that operates by feedback from the EFR rotor speed ω_r and torque T_r. The algorithm returns the steady-state system information, giving the equilibrium values for the speeds of the armature ω_a^* (that goes to the displacement controller) and of the rotating field ω_i^* (that goes to the VSC frequency controller). This last parameter is transformed via PWM into an appropriate electric signal that, in the end, manifests at the EFR as a rotor speed ω_r and as a torque T_r delivered to the generator — and feedbacks the Slip algorithm.

4. THE TWOFOLD CONTROL STRATEGY

4.1 Feedback Linearization

Let a first-order differential equation in time domain be given by $\dot{y} = f + gu$, where y is a variable to be controlled, f and g are continuous functions and u is a signal defined by a control law to be implemented by a feedback routine (Franklin et al., 2013). The control system aims to make y attain a desired value y^*, or, equivalently, to have the error $\varepsilon = y - y^* \to 0$ as $t \to \infty$.

Decisive for that success, the control law must be sufficiently well designed. The feedback linearization approach usually employs a first-order control law:

$$u = \frac{-f + \dot{y}^* - \kappa\varepsilon}{g}, \tag{20}$$

where $\kappa > 0$ is an arbitrary real number. Once the law (20) is substituted in the expression of $\dot{y}$, it gives

$$\begin{aligned} \dot{y} &= f + g\,\frac{-f + \dot{y}^* - \kappa\varepsilon}{g} \\ &= \dot{y}^* - \kappa\varepsilon. \end{aligned} \tag{21}$$

But $\dot{y} - \dot{y}^* = \dot{\varepsilon}$, implying $\dot{\varepsilon} + \kappa\varepsilon = 0$, a linear ODE whose general solution is $\varepsilon = \varepsilon_0\,\mathrm{e}^{-\kappa t}$. Therefore, at each time t_k the controller updates the signal y_k according to the control law (20), the output y_{k+1} approximates to y^* with an error that converges exponentially to zero.

4.2 Application to the Control of the Motor's Displacement

Substituting the expression for the armature torque (1) in (4) and solving for $\dot{\omega}_a$ gives the angular acceleration

$$\dot{\omega}_a = \frac{\eta_m d\Delta p - T_e - B_a\omega_a}{J_a}. \tag{22}$$

Putting (22) in the form $\dot{y} = f + gu$ gives the identities: $y = \omega_a$, $\dot{y}^* = 0$ (because a steady state is desired), and: $u = d'$ (prime means future value), $g = \eta_m\Delta p/J_a$ and $f = -\left(T_e + B_a\omega_a\right)/J_a$. The resulting control law for the displacement, by (20), is:

$$d' = \frac{T_e + B_a\omega_a - J_a\kappa_{\mathrm{M}}\left(\omega_a - \omega_a^*\right)}{\eta_m\Delta p}. \tag{23}$$

Thus, the expression above means that the controller must update the displacement in function of, basically, two variables: the electromagnetic torque T_e and the instant angular speed ω_a. Parameters like B_a, J_a, Δp and κ_{M} are treated as constants, and the steady-state speed ω_a^* comes from the Slip algorithm.

However, this equation needs to be put in a more tractable way. According to (1), the denominator term $\eta_m\Delta p$ can be substituted by T_a/d, so if this d goes to the left side of (23), a dimensionless fraction d'/d will result. One can thus rewrite (23) and interpret it as a ratio between future (d') and present (d) displacements:

$$\frac{d'}{d} = \frac{T_e + B_a\omega_a - J_a\kappa_{\mathrm{M}}\left(\omega_a - \omega_a^*\right)}{T_a}. \tag{24}$$

4.3 Control of the Angular Frequency of the Rotating Field

Let $\omega_i^k = \omega_i\left(t_k\right)$ be the angular speed of the rotating electromagnetic field at instant t_k. Let ω_i^* be the steady-state value of ω_i brought by the Slip algorithm. A first alternative would be to make the future ω_i equal to its predicted steady-state value: $\omega_i' = \omega_i^*$, but this might cause sudden slip changes. However, one can circumvent this by emulating feedback linearization through the exponential:

$$\omega_i' = \omega_i^* + \left(\omega_i^k - \omega_i^*\right)\exp\left[-\kappa_i\left(t - t_k\right)\right]. \tag{25}$$

While both input and loading conditions do not change, ω_i^* remains constant and the field rotation converges smoothly: $\omega_i' \to \omega_i^*$. When the load or the wind speed changes at a later time t_ℓ, t_m, ..., the algorithm recalculates ω_i^* and the process is repeated. Fig. 6 illustrates the point.

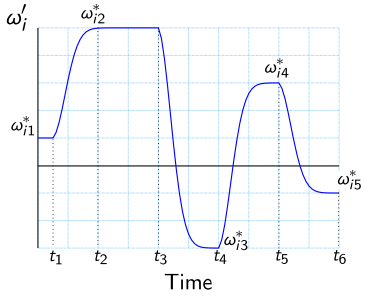

Figure 6: A way to control the speed of the rotating field: every time the load or the wind speed changes, the Slip algorithm updates ω_i^* and the controller makes the future speed ω_i' converge exponentially to it

5. SIMULATION

This work chose as design reference conditions: (1) Wind power delivered to the armature: $P_a = 4\,\mathrm{kW}$; (2) Rotor load: $P_r = 5\,\mathrm{kW}$. The EFR 01-prototype dataset (Table 1) was used as source of input parameters. The Slip algorithm was applied to the numbers, predicting for the steady state: $s^* = 0.0148$, $\omega_a^* = 99.6\,\mathrm{rad/s}$ and $\omega_i^* = 26.5\,\mathrm{rad/s}$.

Table 1: EFR Parameters†

Mechanical Quantities		Electrical Quantities	
$J_a\,(\mathrm{kg\cdot m^2})$	0.0664084 [a]	$R_1\,(\Omega)$	0.66209
$J_r\,(\mathrm{kg\cdot m^2})$	0.501953 [b]	$R_2\,(\Omega)$	0.609071
$B_a\,(\mathrm{W\cdot s^2/rad^2})$	0.003445	$R_m\,(\Omega)$	108.28112
$B_r\,(\mathrm{W\cdot s^2/rad^2})$	0.00028589	$X_1^0\,(\Omega)$	0.7096819
		$X_2^0\,(\Omega)$	0.7096819
		$X_m^0\,(\Omega)$	22.263793
		$\mathrm{pp_{REF}}$	3 [c]
		$\mathrm{pp_G}$	3 [d]
		q	3
		$V\,(\mathrm{V})$	220

† Obtained experimentally (Pinheiro et al., 2019).
[a] Including mass moment of inertia of the hydraulic motor equal to $0.061\,\mathrm{kg\cdot m^2}$.
[b] Including (estimated) mass moment of inertia of the generator equal to $0.5\,\mathrm{kg\cdot m^2}$. [c, d] Design choices for the present study.

The overall efficiency η of a hydraulic machine is usually defined as the product of a volumetric efficiency η_v (which is a ratio of ideal and real volumes of fluid driven per revolution) and a mechanical efficiency η_m (which is a ratio

of real and ideal output torques). Assuming for the motor: $\eta_v = \eta_m = 0.95$, it results $\eta = 0.90$. Some steady-state parameters can be calculated with that:

(1) Motor input power: as the armature receives P_a from the motor, the motor receives from the pump an amount P_h of hydraulic power equal to P_a/η, giving 4.43 kW.
(2) Flow rate in the hydraulic circuit: adopting $\Delta p = 200$ bar for the pressure load, the flow rate Q is equal to $P_h/\Delta p$, giving $2.22 \times 10^{-4}\,\mathrm{m^3/s}$ or 13.3 L/min.
(3) Motor's displacement: the flow rate Q in a hydraulic motor that rotates at speed ω is defined by $Q = d\omega/\eta_v$; here, ω is the steady-state armature speed, so the steady-state displacement d^* can be written as $d^* = \eta_v Q/\omega_a^*$, giving, in this case, $d^* = 13$ mL/rev.

5.1 The Operation Scenarios

A Scilab program was written to simulate the system behavior in a given range of wind speeds. Two combinations of load and wind power were analyzed (Fig. 7): case 1 deals with constant power levels, whilst generalized case 2 shows a variable load profile with a random oscillation of P_a.

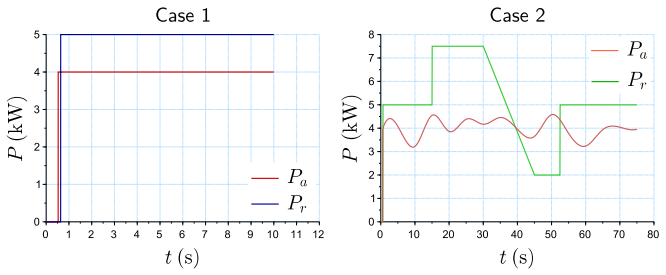

(a) Constant P_a and P_r (b) Random P_a and variable P_r

Figure 7: Power profiles: case studies

The EFR start-up follows the order: (1) start as a conventional motor (armature blocked); (2) rotor stabilization; (3) armature release; (4) coupling to the hydraulic system; (5) control of the armature speed; and (6) control of the rotating field speed.

The rotor accelerates under a balance of electromagnetic, load and friction torques. The load is introduced at an instant t_0 when the rotor movement is sufficiently developed. The criterion adopted here is the maximum torque, when the slip is given (Umans, 2014, p. 363) as

$$s_{\mathrm{maxT}} = \frac{R_2}{\sqrt{R_{1,\mathrm{eq}}^2 + (X_{1,\mathrm{eq}} + X_2)^2}}. \qquad (26)$$

This produces maximum torque difference and maximum initial acceleration. The steady state will be considered "achieved" when $\dot{\omega}_r \leqslant 0.001\,\mathrm{rad/s^2}$.

The armature is then unlocked. Now the objective is to accelerate it up to speed ω_a^* calculated by the Slip algorithm. In order for the acceleration to take place in minimum time, it takes a maximum hydraulic torque to overcome the electromagnetic and frictional torques.

A power transient is expected. There was a registered peak almost 30% higher than the first one. This step is a quick transition to the full EFR regime (that was arbitrated to take place when $\omega_r = 0.1\omega_r^*$), and then ω_i is modified according to the exponential law of (25).

6. RESULTS

Case 1 was simulated with a time step $h = 1/500$ s. For case 2, a smaller $h = 1/4000$ s was necessary, due to the stiffness of the problem: when the coupling occurs, the armature undergoes a strong acceleration that causes a rapid increase in slip. So, the time step has to be short in that region. Table 2 summarizes the numbers.

Table 2: Simulation results

Quantity	Value	
s^*	0.01482	
ω_r^* (rpm)	1200.0	
ω_a^* (rpm)	950.9	
ω_i^* (rpm)	252.8	
P_a^*, P_i^*, P_r^* (kW)	4, 1.05, 5	
	Case 1	**Case 2**
Time step (s)	1/500	1/4000
κ-parameters	$\kappa_i = \kappa_{\mathrm{M}} = 1$	
Simulation time (s)	10	75

In the graphical presentation of the results, the variables will be shown in a generalized per-unit system (p.u.), in the following terms:

- Contrary to the conventional use of adopting a single base unit for all the variables, in this work each variable x will be normalized by its respective steady-state value x^*: *e.g.*, P/P^*, T/T^*, etc.
- The focus here is in following the simultaneous evolution of several quantities towards dynamic equilibrium (when they all assume 1 p.u.), especially the angular speed of the rotor. Naturally, the slip, having no dimensions and varying almost completely (in the context of this simulation) in the range 0 – 1, needs no normalization; however, some graphs show a normalized slip s/s^*.

6.1 Case 1 (Figs. 8a–8f)

The start-up process (0–0.53 s) is the same of a conventional motor, with $\omega_i = 125.7$ rad/s (1200 rpm). The rotor is accelerated to an equilibrium place (733 rpm) which is 61 percent (0.61 p.u.) of the final speed. In the steady state, $\omega_i^* = 28,5$ rad/s (252.8 rpm), so ω_i must decrease and ω_r increase. The armature will be unlocked at the end of phase 1 and ω_a will reach 99.6 rad/s (951 rpm). The angular speed of the rotor drops slightly because the decrease of ω_i is greater than the increase of ω_a and also because of the uplift in s. This will bring about a high power transient. Two peaks must occur: the first, related to the start of the induction motor, and a second one as an effect of the control over ω_a. While the control performs adjustments of ω_a and ω_i, the slip falls down again and all the speeds converge to 1 p.u. The toque curves tend to coincide at equilibrium (as friction is negligible) and the motor's displacement grows rapidly during the coupling, but eventually converges to $d^* = 13$ mL/rev faster than predicted by constant κ_{M}.

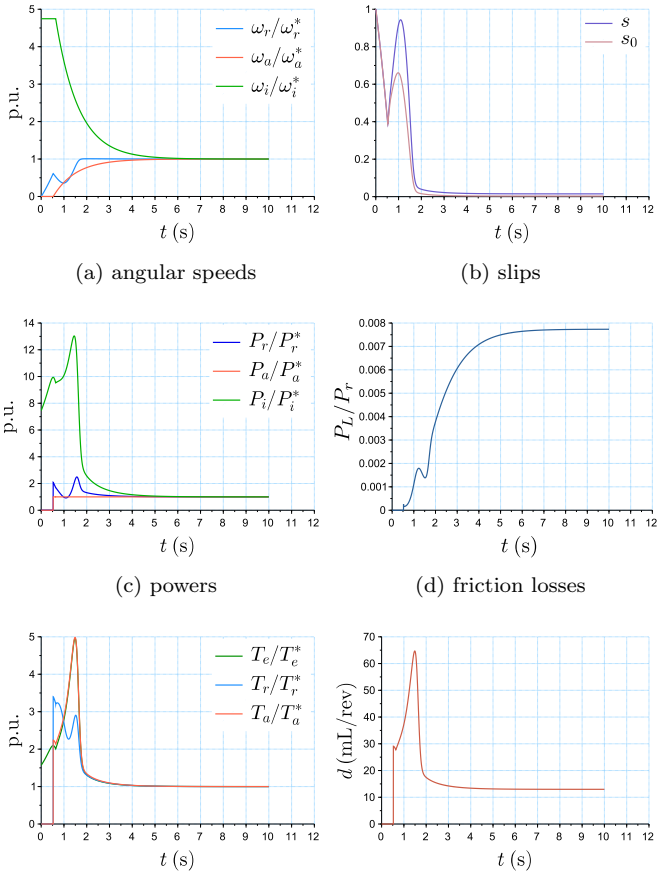

(a) angular speeds (b) slips

(c) powers (d) friction losses

(e) torques (f) motor's displacement

Figure 8: EFR operation: case 1

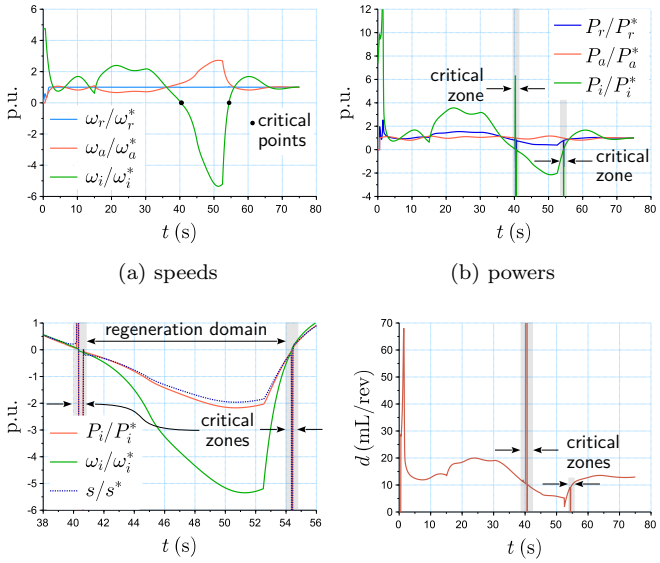

(a) speeds (b) powers

(c) regeneration interval (d) motor's displacement

Figure 9: EFR operation: case 2

6.2 Case 2 (Figs. 9a–9d)

Dynamical Behavior Random changes in turbine rotation will cause variations in the armature torque. Because the electromagnetic torque does not depend linearly on the slip, the response of the VSC may be proportionally greater or less than the variation of P_t, and the armature will suffer high accelerations. This response, however, has been consistent with the hybridization philosophy: the VSC power contribution is positive when $s > 0$ and negative (regeneration) otherwise.

Prohibited Zones Two critical situations can appear: when $\omega_i = 0$ and when $s = 0$. There is no electromagnetic torque in these cases. Such a limitation must be viewed as inherent to the structure of the induction machine.

In this regard, the expedient adopted was, for the first case, to impose $|\omega_i| \geqslant 1\,\text{rad/s}$, and, for the second, to add or remove a small fraction of P_a when $|s^*| < 0.001$ to increase the difference $|P_r - P_a|$. Physically, this corresponds to using an energy-dissipating element or changing the load profile. Naturally, numerical instabilities will arise in the neighborhood of the critical values. This characterizes prohibited zones of service.

To treat the problem, a brake system can be introduced in the EFR/generator interconnection, with a control loop to prevent the slip from falling into the instability regions. Hence, this kind of problem demands a preditive, dedicated control. The feedback linearization approach is not sufficient for this particular situation, for the present control stategy is based on an approximation error ε without taking into account the singularity condition.

7. CONCLUSIONS

The start-up and operation of the EFR were simulated in two scenarios of different profiles of wind speed and load. The simulation indicated that the EFR was able to complement the turbine power to supply the required load with battery assistance; and, in case of excessive wind power, it performed energy regeneration into the battery without compromising neither the load level nor the rotor speed. This adds new features to the wind turbine:

(1) The EFR ensures fast and efficient control of the generator shaft speed, keeping it constant regardless of the wind speed variations;
(2) The EFR brings a positive innovation to the quality of energy delivered by wind power systems by providing voltage free of harmonic distortions, as well as stable torque and power at the generator input. This also affects DC systems (like batteries or PV panels) that connect to the grid via electronic inverters.
(3) There is a concrete possibility of hybridization: over-dimensioned projects can make the EFR operate in regeneration mode, directing wind power to both the generator and the battery. The stored energy can be consumed in periods of low wind activity in a manner transparent to the load. These conclusions can be extrapolated to other situations involving energy regeneration, like electric vehicles. Furthermore, the hybrid system can be designed so that the generator permanently operates very close to its rated power, which contributes to a capacity factor of $\approx 100\%$.

REFERENCES

Costa, D.A.d., Pinheiro, R.F., and Medeiros Jr., M.F.d. (2016a). Dimensionamento e Diretrizes para o Despacho

da Geração de um SHGE Acoplado Através de Regulador Eletromagnético de Frequência. In *VI Brazilian Symposium of Electrical Systems — May 22–25*. Natal. doi:10.20906/CPS/SBSE2016-0389.

Costa, D.A.d., Pinheiro, R.F., and Medeiros Jr., M.F.d. (2016b). Sistema Híbrido de Geração de Energia Elétrica Conectado à Rede, Incluindo o Regulador Eletromagnético de Frequência — REF. In *VI Brazilian Congress on Solar Energy — Apr 04–07*. Belo Horizonte. URL https://www.abens.org.br/CBENS2016/anais/anais/trabalhos/26570final.pdf.

Delft University of Technology (2020). *Hydraulic Wind Turbines*. URL https://www.tudelft.nl/en/3me/about/departments/delft-center-for-systems-and-control/research/data-driven-control/hydraulic-wind-turbines.

Flesch, E.A. (2012). *Projeto de transmissão hidrostática para aerogeradores de eixo horizontal*. Master's thesis, Universidade Federal de Santa Catarina, Brazil. URL http://repositorio.ufsc.br/xmlui/handle/123456789/100954.

Franklin, G.F., Powell, J.D., and Emami-Naeini, A. (2013). *Sistemas de Controle para Engenharia*. Bookman, Porto Alegre, 6th edition.

Freitas Nunes, E.A.d. (2021). *Contribuições para a Estratégia de Controle Aplicadas ao Regulador Eletromagnético de Frequência (REF)*. Ph.D. thesis, Universidade Federal do Rio Grande do Norte, Natal, Brazil. URL https://repositorio.ufrn.br/handle/123456789/32751.

Frøyd, L. (2009). *Control System on a Wind Turbine: Evaluation of Control Strategies for a Wind Turbine with Hydraulic Drive Train by Means of Aeroelastic Analysis*. Master's thesis, Norwegian University of Science and Technology. URL http://hdl.handle.net/11250/235526.

Pinheiro, R.F., Costa Jr., N., and Silva, P.V. (2021). Aerogerador de velocidade variável e tensão e frequência constantes com regulação eletromagnética de frequência - Patente BR nº 102014005059-0.

Pinheiro, R.F., de Souza, D.S., de Carvalho Alves Pessoa, G.A.P., Freitas Nunes, E.A.d., and Souza, F.E.C. (2019). Medição dos parâmetros de circuito equivalente, através de ensaios de curto-circuito e circuito aberto. Unpublished work.

Ramos, T.A.d.O., Medeiros Jr., M.F.d., Pinheiro, R.F., and Medeiros, A. (2019). Slip control of a squirrel cage induction generator driven by an electromagnetic frequency regulator to achieve the maximum power point tracking. *Energies*, 2100(12). doi:10.3390/en12112100.

Ramos, T.A.d.O. (2019). *Um Sistema Eficiente de Máquinas Elétricas para Geração de Energia Eólica com Acionamento por meio de um Regulador Eletromagnético de Frequência*. Ph.D. thesis, Universidade Federal do Rio Grande do Norte, Natal, Brazil. URL https://repositorio.ufrn.br/jspui/handle/123456789/28472.

Silva, J.C.L.d., Ramos, T., and Medeiros Jr., M.F.d. (2021). Modeling and harmonic impact mitigation of grid-connected SCIG driven by an electromagnetic frequency regulator. *Energies*, 14(15). doi:10.3390/en14154524.

Silva, P.V. (2015). *Regulador Eletromagnético de Frequência aplicado no controle de velocidade de geradores eólicos*. Ph.D. thesis, Universidade Federal do Rio Grande do Norte, Natal, Brazil. URL https://repositorio.ufrn.br/handle/123456789/20227.

Silva, P.V., Pinheiro, R.F., Salazar, A.O., Santos Jr., L.P., and Azevedo, C.C.d. (2015a). A proposal for a new wind turbine topology using an electromagnetic frequency regulator. *IEEE Latin America Transactions*, 13(4). doi:10.1109/TLA.2015.7106347.

Silva, P.V., Pinheiro, R.F., Salazar, A.O., and Fernandes, J.D. (2015b). Performance analysis of a new system for speed control in wind turbines. In *ICREPQ'15 – International Conference on Renewable Energies and Power Quality*. doi:10.24084/repq13.356.

Silva, P.V., Pinheiro, R.F., Salazar, A.O., Santos Jr., L.P.d., and Fernandes, J.D. (2015c). Um novo sistema para controle de velocidade em aerogeradores utilizando o Regulador Eletromagnético de Frequência. *Revista Eletrônica de Potência*, 20(3), 254–262. doi:10.18618/REP.2015.3.2539.

Thomsen, K.E., Dahlhaug, O.G., Niss, M.O.K., and Haugset, S.K. (2012). Technological advances in hydraulic drive trains for wind turbines. *Energy Procedia*, 24, 76–82. doi:10.1016/j.egypro.2012.06.089.

Umans, S.D. (2014). *Máquinas Elétricas de Fitzgerald e Kingsley*. Bookman, 7th edition.

You, R., Barahona, B., Chai, J., and Cutululis, N.A. (2013). A novel wind turbine concept based on an electromagnetic coupler and the study of its fault ride-through capability. *Energies*, 6(11), 6120–6136. doi:10.3390/en6116120. URL https://www.mdpi.com/1996-1073/6/11/6120.